JOURNAL OF THERMOPHYSICS AND HEAT TRANSFER
Vol. 11, No. 2, April–June 1997

Modeling of Room-Temperature Heat Pipe Startup from the Frozen State

J. M. Ochterbeck*
Clemson University, Clemson, South Carolina 29634-0921

An analytical investigation was conducted to examine the effects of noncondensible gas charging on restart from the frozen state for room-temperature heat pipes. The model utilized regional energy balances and assumed uniform regional temperatures, independent movement of the vapor/gas front and the liquid melt front, and working fluid sublimation in the frozen state. The model compared well with experimental data for a uniformly distributed working fluid along with negligible noncondensible gas loading and for sufficient gas charging to result in a gas-controlled restart condition. The analysis showed that for negligible noncondensible gas charges up to 90% of the evaporator heat addition may be carried out of the evaporator by sublimating fluid, thus leaving insufficient heat addition to thaw the heat pipe. For high levels of noncondensible gases, restart was easily accomplished and was gas controlled.

Nomenclature

A = area
C = heat capacity per unit length
c = specific heat per unit length
D = diameter
h = latent heat, heat transfer coefficient
j = mass flux
l, L = length
M = molecular mass
m = mass
$\dot{m}$ = mass transfer rate
P = pressure
Q = heat transfer rate
R = universal gas constant, radius
T = temperature
T^* = transition temperature
t = time
x = axial position
λ = mean free molecular path
ρ = density
σ = accommodation coefficient

Subscripts

a = adiabatic
amb = ambient or sink
ax = axial
c = condenser
e = evaporator
f = fluid, freezeout
g = gas
i = initial
l = liquid
lv = vaporization
mp = melting point
p = pipe, pressure
sat = saturated
sl = fusion
sv = sublimation
v = vapor
w = wick

Presented as Paper 95-0419 at the AIAA 33rd Aerospace Sciences Meeting and Exhibit, Reno, NV, Jan. 9–12, 1995; received July 26, 1995; revision received Nov. 2, 1996; accepted for publication Nov. 18, 1996.

*Assistant Professor, Department of Mechanical Engineering. E-mail: jay.ochterbeck@ces.clemson.edu. Senior Member AIAA.

Introduction

EXISTING experimental data and analytical models of frozen startup have resulted primarily from investigations conducted on liquid metal heat pipes, as liquid metal heat pipes must at one point start from the frozen state.[1] Although heat pipes utilizing room-temperature working fluids, such as water and ammonia, would normally not freeze during standard operation or manufacturing, several situations occur where the freeze/thaw behavior is important, specifically in existing and future spacecraft thermal control systems.[2] Numerous satellites utilize heat pipes as part of the thermal control systems and have demonstrated the ability of heat pipes to operate efficiently in microgravity environments. Additionally, high-capacity heat pipe radiators have been considered for use in large, manned spacecraft thermal control systems. Proposed short-term solutions, such as incorporating auxiliary heaters or secondary heat pipes, inhibit the overall system by adding extra weight, additional costs, and depriving the spacecraft system of valuable power resources.

During startup from the frozen state of liquid metal heat pipes, several periods exist with distinctive processes that affect startup.[3] When free molecular conditions exist throughout the heat pipe, no heat transport in the vapor passage is possible, and only heat transfer by conduction through the heat pipe case and wicking/working fluid structure occurs. This conduction-dominated state remains even after melting of the frozen working fluid is initiated, since no vaporization, and therefore, no vapor heat transport, occurs until continuum vapor flow conditions are achieved. With sufficient heating and time, the working fluid temperature in the evaporator is adequate to sustain continuum vapor flow conditions. However, as the vapor will rapidly condense as it contacts the significantly cooler and/or frozen sections of the heat pipe, free molecular flow conditions remain throughout a significant portion of the heat pipe during the initial starting stages.

In the analysis of frozen startup for room-temperature heat pipes (122–630 K), all reported experiments that have not incorporated noncondensible gas charging have resulted in evaporator dryout during startup.[1] Although several tested frozen heat pipes have been successfully restarted, these instances of startup have involved evaporator dryout followed by evaporator rewetting. Generally, evaporator rewetting resulted only after the condenser heat removal rate was decreased.

Abramenko et al.[4] performed an experimental investigation using a 0.95-m aluminum/ammonia axially grooved heat pipe. Isothermal operation and successful startup occurred only after reducing the condenser heat rejection rate. The decreased heat rejection rate allowed the condenser fluid to melt and rewet the evaporator. Effects of axial wall conduction on frozen restart were found to be negligible. Similar tests conducted using a 0.5-m aluminum/ammonia axially grooved heat pipe and identical operating conditions produced comparable results.[5] Faghri[6] conducted an investigation of frozen startup using a copper/water heat pipe. Successful startup was not obtained with evaporator heat addition in general. One successful startup case was reported, however, which involved pulsed evaporator heat addition and no condenser coolant flow, resulting in negligible condenser heat rejection.

Noting the difficulties in frozen startup in room-temperature heat pipes, an analysis was conducted using a copper/water heat pipe to investigate the freeze/thaw characteristics (thus, the entire thermal history) and effects of noncondensible gas loading.[7–9] The experimental heat pipe was fitted with a transparent cover that allowed direct internal observations of the working fluid. For low levels of gas loading, sublimation and migration of the working fluid were observed during freezing and resulted in restart failure. Increases in gas loading aided restart by blocking the sublimation/migration process and the heat pipe restarted in a gas-controlled mode. To stop the fluid migration for low gas levels and therefore obtain a uniformly distributed working fluid for room temperature fluids, either 1) no temperature variations along the heat pipe must exist, or 2) the heat pipe must be frozen to temperatures significantly below the triple point.

All analytical/numerical models of frozen startup have inherently assumed a uniformly distributed frozen working fluid in the wicking structure. Sockol[10] presented an analytical model for gas-loaded liquid metal heat pipes, where startup was specified to initiate when the magnitude of the working fluid vapor pressure was proportional to the initial gas charge pressure. This model was later used by Ponnappan et al.[11] to predict the transient temperature variations during startup of a composite-wick, gas-loaded, sodium heat pipe. Bystrov and Goncharov[12] presented an analytical investigation for gas-loaded, liquid-metal heat pipes. Numerical investigations have been presented by Bowman,[13] which examined the effects of using two different phase-change criteria in the numerical analysis, and by Jang et al.,[14] which developed a finite element numerical model and incorporated free molecular and continuum flow regimes. A numerical analysis for liquid metal working fluids was performed by Cao and Faghri[3,15] with the entire startup process and transition to steady state being included. Also, Cao and Faghri[16] noted the difficulty in utilizing the previous analyses, as extensive numerical calculations were required; therefore, a closed-form analytical solution based on observations and trends specifically for liquid metal heat pipes was presented.

Overall, the published information addressing modeling of the restart characteristics of heat pipes has been directed toward liquid metal working fluids and for room-temperature heat pipes available modeling information is very limited, thus additional investigation is required. This investigation analytically examines the behavior of frozen startup for room-temperature heat pipes, as startup difficulties have consistently been encountered experimentally for room-temperature working fluids. Also, the effects of utilizing noncondensible gas charging will be examined as previous experimental work has shown gas loading aids frozen startup for both liquid metal and room-temperature heat pipes.

Analysis

Previous investigations of liquid metal heat pipes have demonstrated that prior to continuum vapor flow conditions, heat and mass transfer in the vapor channel is essentially negligible under a free molecular flow regime.[14] Negligible evaporation results from 1) an insufficient vapor pressure to sustain vaporization or 2) from the collision of vapor molecules with the physical boundaries instead of other vapor molecules. In determining the point at which large-scale vaporization from the wicking structure will occur, the transition from free molecular vapor flow to continuum vapor flow must be evaluated. Transition criteria is based on evaluating where the mean free molecular path of the vapor molecules becomes much less than the minimum vapor space dimension, and is given by

$$T^* = (Kn/R)[P_v D/(\rho_v \lambda)] \tag{1}$$

where the product $\rho_v \lambda$ is assumed essentially constant[17] and evaluated by examination of the temperature-dependent viscosity data of individual fluids and $Kn < 0.01$ for continuum vapor flow. The assumption of a constant $\rho_v \lambda$ correlates quite well with vapor viscosity data for liquid metal working fluids, whereas it only correlates moderately well for room temperature working fluids. Only the working fluid vapor pressure–temperature relationship is required to evaluate T^*. For room-temperature working fluids (water and ammonia), continuum flow conditions can be shown to exist for temperatures below the triple state, where the fluid exists in a saturated solid–vapor phase.

Startup Regimes—Initial Continuum Vapor Flow

Since continuum vapor flow conditions for heat pipes utilizing room-temperature working fluids can exist with a frozen working fluid, the startup regimes previously discussed for liquid metal working fluids, which assumed an initially free molecular vapor flow state, must be reassessed for frozen startup with room-temperature working fluids. The corresponding startup regimes with a room-temperature fluid are illustrated in Fig. 1, assuming 1) an initially uniformly distributed working fluid, 2) no noncondensible gases are present, and 3) successful startup.

The primary difference between startup of liquid metal heat pipes and room-temperature heat pipes is the absence of the conduction-dominated regime, which exists in the early periods with free molecular vapor flow conditions, common to liquid metals. Because of a saturated solid–vapor phase and the existence of continuum flow conditions, sublimation of the working fluid is therefore possible and results in heat and mass transport by the working fluid vapor in addition to heat diffusion in the solid regions (Fig. 1a). Because the free molecular regime is no longer present, the condition of melting a significant portion of the working fluid by conduction prior to large-scale vaporization is not found in room-temperature heat pipes. Once the evaporator temperature is increased to the tri-

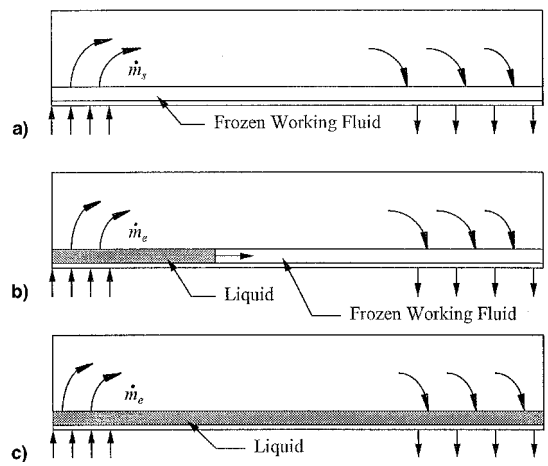

Fig. 1 Frozen startup regimes for initial continuum flow conditions.

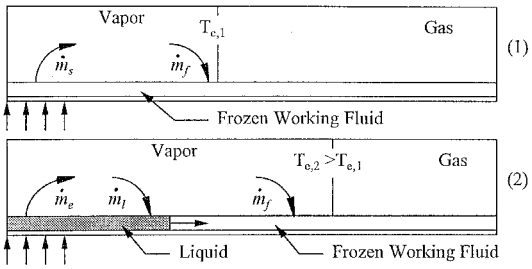

Fig. 2 Schematic of vapor/gas front and melt front during startup.

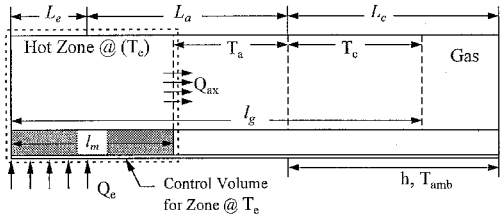

Fig. 3 Schematic of vapor/gas front and melt front locations.

ple point, melting in the wicking structure is initiated and a melt front propagates along the wick with time (Fig. 1b). Eventually, the melt front contacts the far condenser end and the heat pipe responds isothermally to variations in heat transferred/stored (Fig. 1c).

The sublimation and corresponding loss of mass in the evaporator is a direct disadvantage to the restart process for room-temperature heat pipes, since no mass return to the evaporator is possible until the frozen working fluid has melted. Thus, the process of evaporator dryout is always initiated during sublimation regimes. The rate at which the working fluid sublimates is primarily a function of the vapor pressure gradient ΔP_v (related to the rate of change in vapor pressure with respect to temperature, or dP/dT) between the evaporator and condenser ends, the vapor viscosity μ_v, the latent heat of sublimation h_{sv}, and the self-diffusion coefficient, D_{ab} (for very low vapor pressure gradients). To prevent total dryout, the evaporator working fluid inventory must be sufficient to effectively handle the initiation of dryout and allow for melting of the evaporator working fluid along with liquid return to the evaporator. Given the restart difficulties experienced in all previous frozen room-temperature heat pipe investigations, the initial sublimation process appears to significantly affect the restart capabilities.

As initiation of evaporator dryout occurs during sublimation periods and successful startup is directly dependent on the rate of working fluid freezeout, the addition of noncondensible gases may be required for successful startup to control the evaporation/sublimation rate. Figure 2 illustrates this condition schematically. The total mass leaving the evaporator by evaporation/sublimation $\dot{m}_e$ or $\dot{m}_s$, will either condense along the active region containing liquid $\dot{m}_l$, or condense along the frozen region of the wicking structure $\dot{m}_f$, where $\dot{m}_f$ is effectively frozen out and depletes the available inventory.

The effects of noncondensible gas-loaded room-temperature heat pipes can vary significantly from gas-loaded liquid metal heat pipes. During startup of a gas-loaded liquid metal heat pipe, the noncondensible gas initially occupies the entire vapor space under frozen conditions, with this condition prevailing until the vapor pressure $P_v(T_e)$ is equivalent in magnitude to the initial gas pressure P_i. Also, this condition of $P_v(T_e) = P_i$ typically occurs at temperatures well above the working fluid melting point. Further increases in the evaporator temperature and vapor pressure results in the movement of the vapor/gas front and correspondingly, the melt front, along the heat pipe. The movement of the vapor/gas front and melt front essentially propagate at the same rate, thus freezeout of the working fluid is hindered by the noncondensible gas.

However, in a room-temperature heat pipe, the vapor/gas front and the melt front do not necessarily coincide (see Fig. 2). Increases in the evaporator temperature correspond to an increased evaporator vapor pressure that drives the movement of the vapor/gas front, even with a frozen working fluid. The initiation of a melt front within the wicking structure does not occur until the evaporator temperature is greater than the working fluid triple state. The region between the vapor/gas front and the wicking structure melt front allows freezeout of the working fluid to occur. Ensuring proper startup requires the following:

1) The region between the vapor/gas front and liquid melt front is minimal, thus reducing the mass freezeout rate.

2) The evaporator working fluid inventory is sufficient to handle periods of mass freezeout.

Increasing levels of noncondensible gases causes the region between the melt front and the vapor/gas front to be reduced until the two coincide throughout startup with sufficient levels of noncondensible gases.

Frozen Startup Model

The general model developed herein utilizes energy balances applied over the evaporator, adiabatic, and condenser regions, where the temperature in each region is assumed uniform. Common boundary conditions are used to couple the resulting equations (see Fig. 3). Once a melt front l_m has been initiated, the evaporator region is assumed to extend over the region l_m and the temperature over the region l_m is uniform and equal to the evaporator temperature T_e. Once the melt front extends the length of the heat pipe, isothermal operation and response is assumed to occur. The capillary limit within the active region extending over l_m must be evaluated to ensure the internal pressure drops do not exceed the capillary pumping limit.

Modeling of frozen startup for room temperature heat pipes incorporating noncondensible gases must account for a vapor/gas front l_g position and movement that may not coincide with the melt front l_m position in the wicking structure. This condition results from the existence of continuum vapor flow when the working fluid is in the solid state for room-temperature heat pipes. Additionally, because of the existence of continuum vapor flow conditions during the frozen state, sublimation of the working fluid must be included. In formulating the frozen startup model several assumptions are made:

1) The pressure in the vapor channel is constant throughout the heat pipe, or $P_{v,e} = P_{v,c} + P_g$.

2) The axial heat transfer by conduction in the heat pipe case is neglected, as heat transported by vapor governs the transient response.

3) The evaporation/sublimation/condensation rates are uniform over the respective active regions.

4) A one-dimensional front exists at the vapor/gas interface.

5) Mass and heat diffusion through the vapor/gas interface are negligible.

6) The temperatures within prescribed regions are uniform throughout each region.

7) The heat capacity resulting from the latent heat of fusion is linearized over a prescribed temperature interval around the melting point, or $T_{mp} - \delta T < T_{mp} < T_{mp} + \delta T$, where δT was taken to be 0.1 K.

The resulting energy balances are dependent on the location of the vapor/gas front l_g and the location of the melt front l_m, and result in the following:

1) The vapor/gas front is located within the evaporator region, or $l_g < L_e$: The heat input results only in a time rate of change in the evaporator temperature, or

$$c(T_e)L_e \frac{dT_e}{dt} = Q_e(t) \tag{2}$$

where $c(T_e)$ represents the specific heat of the heat pipe per unit length (J/m-K), including the heat pipe case, wicking structure, and the working fluid.

2) The vapor/gas front contacts the adiabatic region, or $L_e < l_g < L_e + L_a$: Heat transfer between the evaporator and adiabatic regions must be included in energy balances for each respective region. The heat transport out of the evaporator region is denoted as $Q_{ax}(t)$, where $Q_{ax}(t)$ corresponds to the heat added to the adiabatic region, and the energy balances for the evaporator and adiabatic regions are, respectively, expressed as the following.

Evaporator region:

$$C_{a-e}\frac{dl_m}{dt} + c(T_e)l_m\frac{d}{dt}(T_e - T_{amb}) = Q_e(t) - Q_{ax}(t) \quad (3)$$

Adiabatic region:

$$C_{amb-a}\frac{dl_g}{dt} + c(T_a)(l_g - L_e)\frac{d}{dt}(T_a - T_{amb}) = Q_{ax}(t) \quad (4)$$

where C_{amb-a} is the total amount of heat per unit length (J/m) required to raise the temperature from T_{amb} to T_a and is later defined mathematically in Eq. (13). The first two terms on the left-hand side of Eq. (3) represent the change in stored internal energy caused by an increase in the melt front location and an increase because of an increased evaporator temperature, respectively. For the case when $T_e < T_{mp}$, the time rate of change dl_m/dt in Eq. (3) is taken to be zero and $l_m = L_e$.

3) The vapor/gas front extends into the condenser region, $L_e + L_a < l_g < L_p$: Heat transfer to the heat sink is possible. Defining the term $[\![A, B]\!]$ as the selection of the greater of A and B, energy balances applied for the evaporator, adiabatic, and condenser regions, respectively, result in the following.

Evaporator region:

$$C_{a(c)-e}\frac{dl_m}{dt} + c(T_e)l_m\frac{d}{dt}(T_e - T_{amb}) = Q_e(t) - Q_{ax}(t) - hP[\![0,\quad l_m - (L_e + L_a)]\!](T_e - T_{amb}) \quad (5)$$

Adiabatic region:

$$c(T_a)[\![0,\quad (L_a + L_e - l_m)]\!]\frac{d}{dt}(T_a - T_{amb}) = Q_{ax,a}(t) \quad (6)$$

Condenser region:

$$C_{c-a(e)}\frac{dl_g}{dt} + c(T_c)(l_g - L_e - L_a)\frac{d}{dt}(T_c - T_{amb}) = Q_{ax,c}(t) - hP(l_g - L_e - L_a)(T_c - T_{amb}) \quad (7)$$

The axial heat transfer exiting the evaporator region or hot zone, $Q_{ax}(t)$, is equal to the sum of the axial heat transfer added to the adiabatic region, $Q_{ax,a}(t)$, and the axial heat transfer added to the condenser region, $Q_{ax,c}(t)$. The axial heat transfer results from the evaporation/sublimation in the evaporator region and mass freezeout in the adiabatic and condenser regions. The portion of the mass evaporated that condenses on the liquid regions of the wick structure is internal to the hot zone control volume and, therefore, does not factor into the presented energy balances. With the assumption of a uniform vapor pressure throughout the vapor channel and that the vapor pressure corresponds to T_e, the mass flux $j(t)$, condensing on the wick in the adiabatic and condenser sections, can be expressed in terms of the pressure difference between the existing vapor channel pressure and the vapor pressure of the saturated frozen fluid in the wicking structure,[18] or

$$j(t) = \left(\frac{2\sigma}{2 - \sigma}\right)\left(\frac{M}{2\pi R}\right)^{1/2}\left\{\frac{P_v(T_e)}{T_e^{1/2}} - \frac{P_v[T_{a(c)}]}{T_{a(c)}^{1/2}}\right\} \quad (8)$$

where σ varies with respect to the working fluid and temperature ranges utilized. The axial heat transport rate added to each section is then determined by integration of the condensing vapor mass flux over the regional surface area, or

$$Q(t)_{ax,a(c)} = \int_A j(t)_{a(c)}h_{sv}\,dA \quad (9)$$

The heat capacity of a heat pipe cross section (J/m-K) includes the heat capacities of the wick, wall, and working fluid, and is given by the following relationships and applicable temperature ranges:

$$c(T) = (A_c c_p)_{case} + A_w[(1 - \phi)c_{p,w} + \phi c_{p,s}] \quad \text{for} \quad (T < T_{mp} - \delta T) \quad (10)$$

$$c(T) = (A_c c_p)_{case} + A_w\left[(1 - \phi)c_{p,w} + \phi\frac{h_{sl}}{2\delta T}\right] \quad \text{for} \quad (T_{mp} - \delta T < T < T_{mp} + \delta T) \quad (11)$$

$$c(T) = (A_c c_p)_{case} + A_w[(1 - \phi)c_{p,w} + \phi c_{p,l}] \quad \text{for} \quad (T > T_{mp} + \delta T) \quad (12)$$

where the latent heat of fusion h_{sl} is linearized over a finite temperature range, $T_{mp} - \delta T < T_{mp} < T_{mp} + \delta T$, and ϕ is the wick porosity. It is important to note that the wick is assumed to be saturated with working fluid in Eqs. (10–12). This has been shown to occur for certain cases only,[7–9] where the modeling of cases of plug formation have been addressed previously.[8,9]

As l_m and/or l_g propagate along the heat pipe, an amount of energy equal to the total heat required to raise the temperature of the cross section from T_1 to T_2, C_{1-2}, must be absorbed by the active region, where C_{1-2} is defined by the relationship

$$C_{1-2} = \int_{T_1}^{T_2} c(T)\,dT \quad (13)$$

and includes the latent heat of fusion h_{sl}, if $T_2 > T_{mp} > T_1$.

Variation of Vapor/Gas Front

The motion of l_g is governed by the evaporator vapor pressure and correspondingly, evaporator temperature T_e. Therefore, a correlation between the vapor/gas front movement and the evaporator temperature rate of change is required. Assuming the vapor and gas behave as perfect gases and no frictional losses are present in the vapor channel, the relationship between the gas front location and the vapor pressure is given by

$$P_v(T_e)L = P_i L_i \quad (14)$$

where P_i and L_i are the initial gas pressure and gas length, respectively, and $L = L_p - l_g$. Figure 4 illustrates these relationships graphically. Differentiating Eq. (14) by d/dt and rearranging results in the relationship

$$\frac{1}{P_v(T_e)}\frac{dP_v(T_e)}{dt} = -\frac{1}{L}\frac{dL}{dt} \quad (15)$$

Since the relationship between the evaporator temperature rate of change dT_e and the vapor/gas front movement dl_g is desired, the Clausius–Clayperon equation

$$\frac{dP_v}{P_v} = \frac{h_{lv}\,dT_e}{RT_e^2} \quad (16)$$

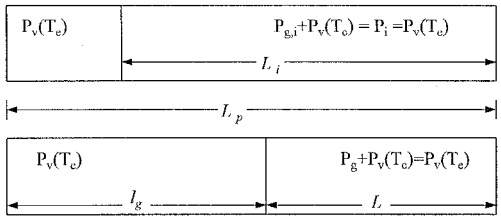

Fig. 4 Relationship between vapor/gas front and internal pressure.

is used to replace dP_v/P_v in Eq. (15). In the case where the evaporator temperature corresponds to a saturated solid–vapor state, h_{sv} is substituted for h_{lv} in Eq. (16). The resulting expression relating the rate of vapor/gas front movement with the rate of evaporator temperature change is given by

$$\frac{dl_g}{dt} = (L_p - l_g)\frac{h_{lv}}{RT_e^2}\frac{dT_e}{dt} \tag{17}$$

and is used to relate the vapor/gas front location and the evaporator temperature given in Eqs. (3–7).

Special Cases of Frozen Startup Model

Two special cases that result in simplification of the previous model may be examined:

1) The heat pipe contains no noncondensible gases.

2) A sufficient noncondensible gas charge is present to result in propagation of l_m and l_g at the same rate. These two cases represent the extreme conditions in terms of freezeout. With no noncondensible gases, maximum freezeout rates will occur, whereas freezeout in the gas-controlled mode is essentially negligible because of a coincident l_m and l_g.

Negligible Noncondensible Gas Charge

In the absence of a noncondensible gas charge, the entire vapor channel space is under continuum vapor flow conditions and maximum freezeout of the working fluid occurs. Using the same basic approach outlined earlier, energy balances over control volumes containing the evaporator, adiabatic, and condenser regions are obtained. An energy balance in the evaporator region results in the expression

$$C_{1-2}\frac{dl_m}{dt} + c(T_e)l_m\frac{dT_e}{dt} = Q_e(t) - Q_{ax}(t) \tag{18}$$

where $l_m = L_e$ until the evaporator region is melted entirely, thus, $dl_m/dt = 0$ for this time interval. The axial heat transport out of the evaporator zone $Q_{ax}(t)$ is the sum of the axial heat transport to the adiabatic region $Q_{ax,a}(t)$, and the axial heat transport to the condenser region $Q_{ax,c}(t)$. For the adiabatic region

$$[\![0,\quad [L_a - (l_m - L_e)]\!]\frac{dT_a}{dt}c(T) = Q_{ax,a}$$
$$= h_{sv}P[\![0,\quad L_a - (l_m - L_e)]\!]j_a \tag{19}$$

Similarly, in the condenser region, an energy balance results in the relationship

$$-[\![-L_c,\ l_m - L_p]\!]c(T)\frac{dT_c}{dt} = Q_{ax,c} - Q_c$$
$$= -[h_{sv}Pj_c - hP(T_c - T_{amb})][\![-L_c,\ l_m - L_p]\!] \tag{20}$$

As stated before, $Q_{ax}(t)$ corresponds to the mass lost caused by freezeout. The total mass lost $m_f(t)$ caused by freezeout in the frozen sections at a given time is found by integrating the relationship

$$m_f(t) = \int_0^t \frac{Q_{ax}(t)}{h_{sv}}\,dt \tag{21}$$

and can be compared to the total evaporator working fluid inventory when determining the depletion of available working fluid in the evaporator during dryout.

Gas-Controlled Startup

Gas-controlled startup corresponds to a specific case where sufficient noncondensible gases are present in the heat pipe to control the melt front (i.e., $l_m = l_g$ throughout startup), and the noncondensible gases are uniformly distributed throughout the heat pipe. As $Q_e(t)$ is applied, the evaporator temperature and vapor pressure will increase, forcing the vapor/gas front out of the evaporator region because of increasing pressure. For the vapor/gas front to effectively control the melt front rate and to prohibit mass lost by freezeout, the evaporator working fluid must be in a liquid state as the vapor/gas front exits the evaporator. The time required for the evaporator temperature to be increased from T_i to T is determined by integrating the relationship

$$c(T_e)L_e\frac{dT_e}{dt} = Q_e(t) \tag{22}$$

and assuming a constant evaporator heat input Q_e, yields upon integration

$$t = \frac{C_{amb-e}L_e}{Q_e} \tag{23}$$

where C_{amb-e} represents the total amount of energy absorbed, including the latent heat of fusion h_{sl}, to raise the evaporator temperature from T_{amb} to T_e and is given by Eq. (13).

The temperature T_e that corresponds to a vapor/gas front located at the evaporator exit is determined using the assumption of an ideal gas compression in the gas-blocked region, or

$$P_v(T_e) = \frac{[P_{g,i} + P_v(T_c)]L_p}{L_c + L_a} = P_g + P_v(T_c) \tag{24}$$

Once the vapor/gas front and the melt front are coincident at the evaporator exit, progression along the pipe will be governed by the melt front rate of change dl_m and the hot zone temperature rate of change dT_e. An energy balance applied over a control volume containing the vapor yields

$$C_{amb-e}\frac{dl_m}{dt} + c(T_e)l_m\frac{d}{dt}(T_e - T_{amb})$$
$$= Q_e(t) - hP[\![0,\ l_m - (L_e + L_a)]\!](T_e - T_{amb}) \tag{25}$$

where the two terms on the left-hand side represent the change in the stored energy of the hot zone because of the advancement of dl_m and the increase in dT_e, respectively.

As $l_g = l_m$ throughout startup, the rate of change of the vapor/gas and melt fronts are equal, thus, using Eq. (17), and substituting $l_m = l_g$ yields the expression relating dl_m and dT_e

$$\frac{dl_m}{dt} = (L_p - l_m)\frac{h_{lv}}{RT_e^2}\frac{dT_e}{dt} \tag{26}$$

Substituting Eq. (26) into Eq. (25), and simplifying, an expression for the time rate of change dT_e/dt is given by

$$\frac{dT_e}{dt} = \frac{Q_e(T_e) - hP[\![0,\ l_m - (L_e + L_a)]\!](T_e - T_c)}{C_{amb-e}(L_p - l_m)(h_{lv}/RT_e^2) + c(T_e)l_m} \tag{27}$$

with the initial condition of T_e is found from Eqs. (22) and (24). Equations (26) and (27) may be simultaneously integrated to determine T_e and l_m.

Capillary Pumping Limit

During startup, the capillary pumping limit in the active hot-zone region, where the wicking structure contains a liquid state working fluid, must not be exceeded or the liquid mass flowrate to the evaporator will decrease below the required mass flowrate, and evaporator dryout will result. The capillary limit is defined such that the maximum capillary pressure in the wick must be greater than the sum of the vapor pressure losses, the liquid pressure losses, axial hydrostatic pressure losses, and perpendicular hydrostatic pressure losses. Using standard heat pipe analysis methods[19] the capillary limit is continuously verified within the hot-zone region to ensure that dryout does not result from exceeding the capillary pumping capabilities.

Results

The analytical model presented herein is compared with experimental data obtained for a 2.0-m copper/water heat pipe that has been described previously in detail.[7–9] The heat pipe has an internal square cross section with sides of 2.54 cm and a copper screen mesh wicking structure. Evaporator heat addition was supplied by an electric heater and condenser heat rejection utilized a circulating cooling fluid, with evaporator and condenser lengths of 0.58 and 0.74 m, respectively. The effects of noncondensible gas charging and thermal history were studied in detail, with gas charges (air) between 0.1225–1.300 cm^3 (at STP) examined. These noncondensible gas levels corresponded to blocked condenser levels between 7–45% when the heat pipe was operating at 160 W and a coolant temperature of −10°C. The analytical results were determined by numerical integration of the appropriate set of equations listed previously, with the error associated with the numerical integration estimated to be no greater than 1–2%. The experimental uncertainties for temperature and power input were listed as ±0.3°C and ±1.0 W.[7]

The initial case examined is for a low gas level of 0.1225 cm^3. The heat pipe was frozen such that an evenly distributed frozen working fluid existed prior to restart. An evaporator heat input of 30 W was initially tested, with the transient liquid temperature measurements for this restart case presented in Fig. 5. As shown, evaporator dryout resulted since the working fluid along the liquid channel remained frozen and could not be pumped back to the evaporator. As heat was applied to the evaporator, the solid layers along the condenser side walls were increased slightly in thickness, because of the working fluid freezeout from the evaporator.

The effects of freezeout for the previous test can be seen by comparing the experimental data with the analytical model (see Figs. 6 and 7). This restart case was modeled using the special

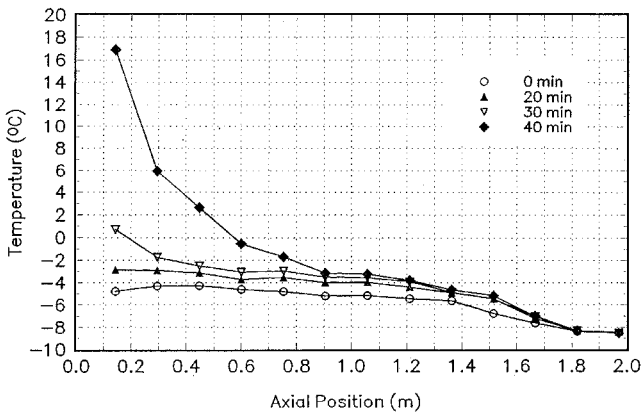

Fig. 5 Restart liquid channel temperatures for 0.1225-cm^3 gas charge, 30-W heat input.

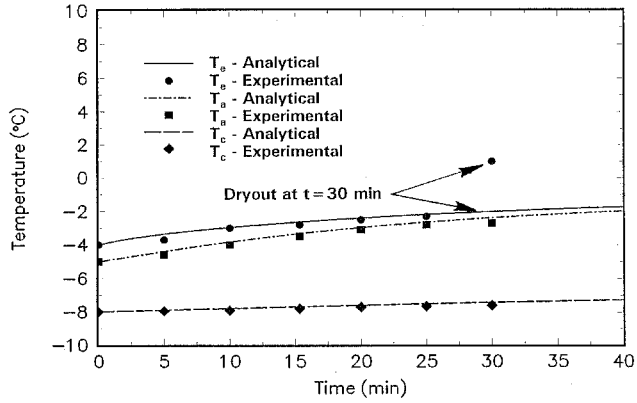

Fig. 6 Analytical/experimental comparison with 0.1225-cm^3 gas charge, 30-W heat input.

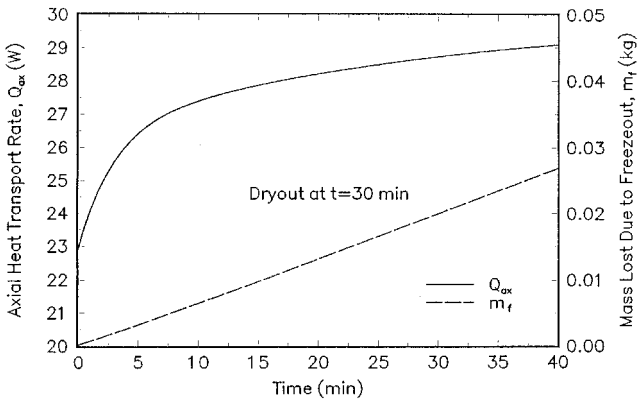

Fig. 7 Axial heat transport and mass freezeout for 0.1225-cm^3 gas charge, 30-W heat input.

case of no noncondensible gases, as an analysis of the vapor/gas front position showed that l_g is a weak function of the internal vapor pressure, thus, $dl_g/dt = 0$. The experimental data presented represent average regional temperatures within the evaporator, adiabatic, and condenser sections. As seen in Fig. 6, the variation in temperature with respect to time is quite low, with dryout experimentally occurring at an elapsed time of 30 min. More interesting is the examination of $Q_{ax}(t)$, and $m_f(t)$, shown in Fig. 7. As the evaporator temperature increases, the vapor pressure correspondingly increases. This causes an increased sublimation rate from the evaporator that carries up to 90% of the applied heat (30 W) out of the evaporator region, thus prohibiting melting of the working fluid as little heat remains to increase the evaporator section temperature. The calculated mass lost at the time of dryout (30 min) m_f represents approximately 40% of the actual available evaporator mass, 0.05 kg. Although the evaporator was not completely dry, experimental dryout was defined as the point where the first liquid channel temperature rose sharply in comparison to the adjacent liquid channel temperatures, thus the mass lost because of freezeout was supplied by the far evaporator region, as is the typical characteristic for evaporator dryout.

Similar startup difficulties were obtained for an evaporator heat input of 80 W for a noncondensible gas charge of 0.1225 cm^3 and a uniformly distributed working fluid (see Figs. 8 and 9). Figure 8 presents the experimental regionally averaged data and comparison with the analytical model. For this case of 80 W of power input, the evaporator and adiabatic sections are seen to melt prior to evaporator dryout, in contrast to a restart power of 30 W. Evaporator dryout occurred experimentally at an elapsed time of approximately 32 min, where dryout is again demonstrated by a rapid increase in the evaporator temperature. Similarly, a corresponding decrease in the condenser temperature, caused by the discontinuation of thermal coupling

of the two regions by vapor transport, is observed. Intuitively, evaporator dryout for the increased power input of 80 W (dryout at 32 min) should occur in a more rapid time than for the power input of 30 W (dryout at 30 min). However, since the evaporator and adiabatic sections in the 80-W restart case were in a liquid state for a large period of time, liquid from the adiabatic section could be pumped into the evaporator, thus, increasing the available mass inventory and delaying the dryout process.

Examination of $Q_{ax}(t)$ and $m_f(t)$ (see Fig. 9), shows the same basic trends as those in Fig. 7. As the evaporator temperature increases, the vapor pressure correspondingly increases. This causes an increased sublimation/evaporation rate from the evaporator that carries up to 90% of the applied heat (80 W) out of the evaporator region. The calculated mass lost at time of dryout (32 min) m_f is approximately equal to the actual available evaporator mass of 0.05 kg. However, as discussed earlier, liquid could be fed to the evaporator from the adiabatic section because of a melted state in both regions.

The liquid channel temperatures for the restart with a 1.248-cm^3 gas charge are presented in Fig. 10. A restart power input of 160 W was utilized, since an instantaneous full restart power would result in the most severe transient possible. As the wick in the evaporator and adiabatic regions was primed with liquid and the vapor channel was not completely blocked, restart was accomplished with the melt front in the condenser wicking structure proceeding frontally. The temperature profiles are consistent and indicative of the frontal heating mode characteristic of startup in gas-loaded heat pipes. In contrast to restart with low noncondensible gas levels in room temperature heat pipes, the movement of the gas/vapor front was found to govern the melt front rate in the wicking structure. This determination resulted from visual observation of the gas/vapor front and the measured liquid channel temperatures, as the location of the fine mist on the lexan cover and a 0°C liquid channel temperature measurement coincided throughout restart.[7]

As the previous test corresponded to a gas-controlled restart, the analytical model results for determining the melt front location l_m and the evaporator temperature T_e, are presented in Fig. 11 along with the average experimental evaporator temperature and the location of the melt front in the liquid channel. As seen, the model and the data are in good agreement. A second restart case for a 1.248-cm^3 gas charge is shown in Fig. 12 for step function power increments between 30–160 W.

For intermediate levels of noncondensible gas charging, a phenomenon, referred to as freezing blowby, was found to occur during restart. This phenomenon for the copper/water heat pipe has been previously examined, both experimentally and analytically, in detail.[8]

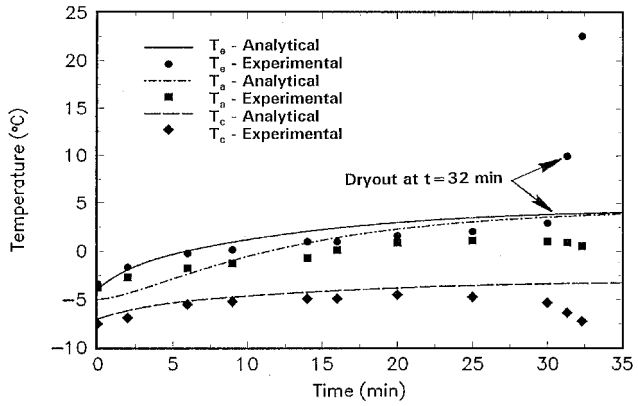

Fig. 8 Analytical/experimental comparison for 0.1225-cm^3 gas charge, 80-W heat input.

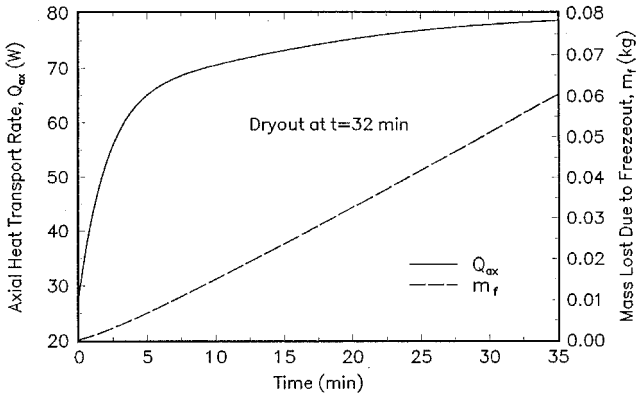

Fig. 9 Axial heat transport and mass freezeout for 0.1225-cm^3 gas charge, 80-W heat input.

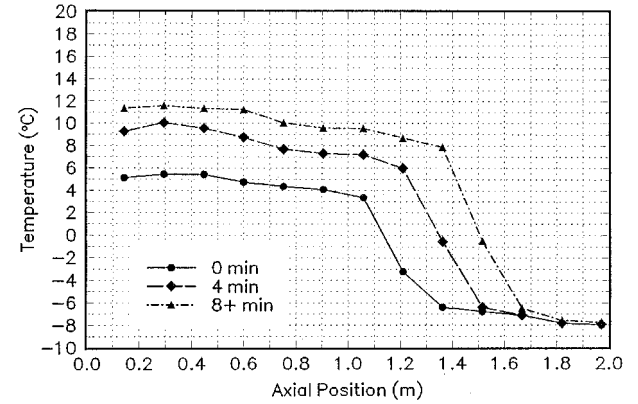

Fig. 10 Liquid channel temperatures for 1.248-cm^3 gas charge, 160-W heat input.

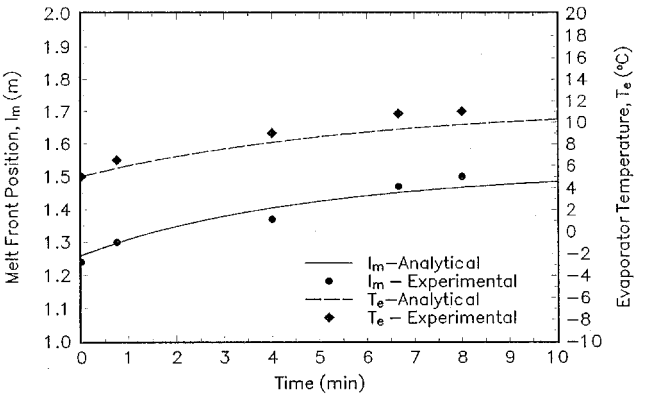

Fig. 11 Gas-controlled restart for 1.248-cm^3 gas charge, 160-W heat input.

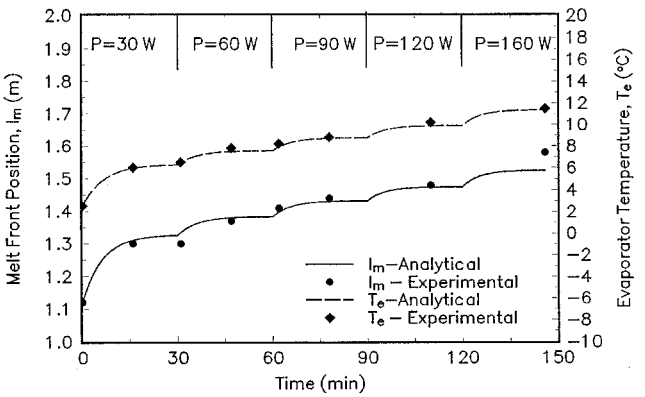

Fig. 12 Gas-controlled restart for 1.248-cm^3 gas charge, step function power increments.

Conclusions

A one-dimensional, transient analysis utilizing regional energy balances in the evaporator, adiabatic, condenser sections was conducted on restart of a gas-loaded room temperature heat pipe. The model assumed a uniformly distributed working fluid and allowed for variations in the vapor/gas front, liquid channel melt front, and sublimation of the working fluid in the frozen state. Additionally, the vapor/gas front and liquid melt front were allowed to vary independently, as the vapor pressure for room temperature heat pipes is sufficient to affect the vapor/gas front motion while in a saturated solid–vapor state, unlike liquid metal working fluids.

Two limiting cases of the analytical model were examined and compared well with experimental data: 1) absence of noncondensible gases and 2) sufficient noncondensible gases to result in a coincident vapor/gas front and liquid melt front, with simultaneous propagation of the two fronts. For the case with no noncondensible gases, sublimation and mass freezeout were sufficient to result in restart failure. The analytical model showed that up to 90% of the evaporator heat input during restart may be transported out of the evaporator by sublimated working fluid, thus, preventing the evaporator wicking structure from melting, and resulting in a significant amount of frozen-out fluid in the condenser region. For room-temperature heat pipes without noncondensible gas charging, dryout of the evaporator always initiates prior to melting of the frozen wicking structure. Thus, the sublimation process has been shown experimentally and analytically to be detrimental to frozen heat pipe startup. With levels of noncondensible gas sufficient to result in a melted evaporator as the vapor/gas front exists the evaporator region, the restart characteristics are gas controlled. The analytical model and experimental data demonstrated successful restart in the gas-controlled mode.

Ensuring restart by evaporator heat addition of a frozen room temperature heat pipe is seen to require the addition of non-condensible gases to reduce mass freezeout rates. If noncondensible gas charging is not possible, the evaporator working fluid inventory must be sufficient to increase the entire heat pipe temperature above the working fluid triple state, in addition to a negligible condenser heat rejection rate to effectively reduce mass freezeout levels.

Acknowledgments

The author would like to acknowledge the support of the NASA Center for Space Power and the South Carolina Space Grant Consortium.

References

[1]Ochterbeck, J. M., and Peterson, G. P., "Current Status of Frozen Heat Pipe Startup Research," *Heat Transfer 1994*, Vol. 7, Chameleon Press, London, 1994, pp. 351–356.

[2]Antoniuk, D., and Edwards, D. K., "Depriming of Arterial Gas-Controlled Heat Pipes," *Proceedings of the 7th International Heat Pipe Conference* (Minsk, Russia), 1990.

[3]Cao, Y., and Faghri, A., "Simulation of the Early Startup Period of High Temperature Heat Pipes from the Frozen State by a Rarefied Vapor Self-Diffusion Model," *Journal of Heat Transfer*, Vol. 115, No. 1, 1993, pp. 239–246.

[4]Abramenko, A. N., Kanonchik, L. E., and Prokhorov, Y. M., "Start-Up Dynamics of an Arterial Heat Pipe from the Frozen or Chilled State," *Journal of Engineering Physics (Inzhenerno-Fizicheskii Zhurnal)*, Vol. 51, No. 5, 1986, pp. 1283–1288.

[5]Vasiliev, L. L., and Kanonchik, L. E., "Dynamics of Heat Pipe Start-Up from a Frozen State," A. V. Luikov Heat and Mass Transfer Inst., Minsk, Belarus, 1993.

[6]Faghri, A., "Frozen Start-Up Behavior of Low-Temperature Heat Pipes," *International Journal of Heat and Mass Transfer*, Vol. 35, No. 7, 1992, pp. 1681–1694.

[7]Ochterbeck, J. M., and Peterson, G. P., "Visualization of the Freeze/Thaw Characteristics of a Copper/Water Heat Pipe: Effects of Non-Condensible Gas Charging, *Journal of Thermophysics and Heat Transfer*, Vol. 7, No. 1, 1993, pp. 127–132.

[8]Ochterbeck, J. M., and Peterson, G. P., "Investigation of the Freezing Blowby Phenomenon in Heat Pipes," *Journal of Thermophysics and Heat Transfer*, Vol. 9, No. 2, 1995, pp. 314–321.

[9]Ochterbeck, J. M., "Freeze/Thaw Characteristics of Room Temperature Heat Pipes—Incorporating Thermal History Effects and Non-Condensible Gas Charging," Ph.D. Dissertation, Texas A&M Univ., College Station, TX, Aug. 1993.

[10]Sockol, P. M., "Startup Analysis for a High-Temperature Gas-Loaded Heat Pipe," NASA TM X-2840, July 1973.

[11]Ponnappan, R., Boehman, L. I., and Mahefkey, E. T., "Diffusion-Controlled Startup of a Gas-Loaded Liquid-Metal Heat Pipe," *Journal of Thermophysics and Heat Transfer*, Vol. 4, No. 3, 1990, pp. 332–340.

[12]Bystrov, P. I., and Goncharov, V. F., "Starting Dynamics of High-Temperature Gas-Filled Heat Pipes," *High Temperature (USA)*, Vol. 21, No. 6, 1983, pp. 927–936.

[13]Bowman, W., "Transient Heat-Pipe Modeling, the Frozen Start-Up Problem," AIAA Paper 90-1773, June 1990.

[14]Jang, J. H., Faghri, A., Chang, W. S., and Mahefkey, E. T., "Mathematical Modeling and Analysis of Heat Pipe Start-Up from the Frozen State," *Journal of Heat Transfer*, Vol. 112, Aug. 1990, pp. 586–594.

[15]Cao, Y., and Faghri, A., "A Numerical Analysis of High-Temperature Heat Pipe Startup from the Frozen State," *Journal of Heat Transfer*, Vol. 115, Feb. 1993, pp. 247–254.

[16]Cao, Y., and Faghri, A., "Closed-Form Analytical Solutions of High-Temperature Heat Pipe Startup and Frozen Startup Limitation," *Journal of Heat Transfer*, Vol. 114, Nov. 1992, pp. 1028–1035.

[17]Zucrow, M. J., and Hoffman, J. D., *Gas Dynamics*, Wiley, New York, 1976.

[18]Collier, J. G., *Convective Boiling and Condensation*, 2nd ed., McGraw–Hill, New York, 1981.

[19]Chi, S. W., *Heat Pipe Theory and Practice*, Hemisphere, Washington, DC, 1976.